Role of Actin Cortex in the Subplasmalemmal Transport of Secretory Granules in PC-12 Cells

Thorsten Lang,* Irene Wacker,[†] Ilse Wunderlich,[†] Alexander Rohrbach,[‡] Günter Giese,[†] Thierry Soldati,[†] and Wolfhard Almers[§]

*Max-Planck-Institut für biophysikalische Chemie, D-37077 Göttingen, Germany; [†]Max-Planck-Institut für medizinische Forschung, D-69120 Heidelberg, Germany; [‡]European Molecular Biology Laboratory, D-69012 Heidelberg, Germany; and [§]Vollum Institute, Portland, Oregon 97201-3098 USA

ABSTRACT   In neuroendocrine PC-12 cells, evanescent-field fluorescence microscopy was used to track motions of green fluorescent protein (GFP)-labeled actin or GFP-labeled secretory granules in a thin layer of cytoplasm where cells adhered to glass. The layer contained abundant filamentous actin (F-actin) locally condensed into stress fibers. More than 90% of the granules imaged lay within the F-actin layer. One-third of the granules did not move detectably, while two-thirds moved randomly; the average diffusion coefficient was 23×10^{-4} μm^2/s. A small minority ($<$3%) moved rapidly and in a directed fashion over distances more than a micron. Staining of F-actin suggests that such movement occurred along actin bundles. The seemingly random movement of most other granules was not due to diffusion since it was diminished by the myosin inhibitor butanedione monoxime, and blocked by chelating intracellular Mg^{2+} and replacing ATP with AMP-PNP. Mobility was blocked also when F-actin was stabilized with phalloidin, and was diminished when the actin cortex was degraded with latrunculin B. We conclude that the movement of granules requires metabolic energy, and that it is mediated as well as limited by the actin cortex. Opposing actions of the actin cortex on mobility may explain why its degradation has variable effects on secretion.

INTRODUCTION

Eukaryotic cells surround themselves with a dense sheet of F-actin subjacent to the plasma membrane, termed the actin cortex. Although important for the maintenance of cell shape and for cell movement (Stossel, 1993; Mitchison and Cramer, 1996) the actin cortex is likely to hinder the movement of secretory vesicles to the plasma membrane, and that of endocytic vesicles to their processing stations in the cytoplasm. Both exo and endocytosis are basic functions of every eukaryotic cell, yet the motion of vesicular organelles through the actin cortex is not well understood.

In static images obtained by deep-etch electron microscopy, the actin cortex appears dense enough to restrict the movement of vesicles (Nakata and Hirokawa, 1992). Indeed, exocytosis occurs preferentially at surface sites where the actin cortex in adrenal chromaffin cells has gaps (Vitale et al., 1991) and was enhanced in some studies when the actin cortex was thinned with cytochalasin-D (Sontag et al., 1988, but also see Morita et al., 1988). In pancreatic acinar cells, moderate actin depolymerization stimulates exocytosis even without an increase in cytosolic [Ca^{2+}] (Muallem et al., 1995). These and related findings have suggested that the actin cortex is a barrier for granules (Cheek and Burgoyne, 1986; Trifaro and Vitale, 1993) that is partially degraded when stimulation activates actin-severing enzymes.

In contrast to this hypothesis, severe depletion of F-actin inhibits exocytosis in pancreatic acinar cells (Muallem et al., 1995), as if a minimal amount of actin is required to transport granules to the plasmalemma. Several findings suggest that an actin-myosin-based transport step is involved: actin and myosin are required for exocytosis at the base of growing microvilli (Fath and Burgess, 1993) as they are in sea urchin eggs, where the myosin inhibitor butanedione monoxime (BDM) inhibits vesicle recruitment for Ca^{2+}-regulated exocytosis (Bi et al., 1997). In synaptosomes, myosin V binds to synaptic vesicles (Prekeris and Terrian, 1997) and under some conditions myosin V attached to synaptic vesicles can move actin filaments (Evans et al., 1998). Moreover, actin can mediate movement even without myosin. Actin polymerization propels *Listeria* through infected cells (Theriot et al., 1992) and moves pinocytic vesicles into the cytoplasm (Merrifield et al., 1999). Does F-actin hinder or facilitate organelle movement in the cell periphery?

Since secretion studies have given conflicting answers to this question, we used video microscopy to directly monitor the motion of an identified organelle in the actin cortex. Dense-core secretory granules in PC-12 cells were labeled with green fluorescent protein (GFP) (Lang et al., 1997; Burke et al., 1997) and imaged by evanescent field fluorescence microscopy (EFM; Stout and Axelrod, 1989; Steyer et al., 1997; Steyer and Almers, 1999; see also Oheim et al., 1998). This technique readily images single granules with high time resolution in living cells. We confirm that actin filaments can hinder the movement of secretory granules, but also show that actin filaments can mediate movement.

MATERIALS AND METHODS

PC-12 cells (clone 251, Heumann et al., 1983) were cultured as described (Lang et al., 1997). Dense-core granules were labeled by transient transfection with human pro-neuropeptide-Y fused to the N-terminal of GFP-mutII. After transfection (Lang et al., 1997), cells were plated on 20-mm-diameter glass coverslips and used 48 h later. For experiments, coverslips were mounted in an open observation chamber filled with an artificial cytosol containing, in mM: 63 potassium glutamate, 50 K-EGTA, 5 CaCl$_2$, 3.5 MgCl$_2$, 1 K-ATP, 5 glucose, 20 PIPES, pH 7.0. Calculated concentrations of free calcium and free MgATP were [Ca^{2+}] = 0.033 μM, [MgATP] = 0.86 mM. Cells were routinely imaged in this solution for 50 frames at 0.83 Hz (for 1 min) before further treatment. In control experiments cells were next permeabilized by adding 7.5 μM digitonin for 30 s. Digitonin was then removed, and after waiting a further 90 s cells were imaged for 1–2 s at 0.83 Hz. In other experiments, magnesium was withdrawn and ATP replaced with a nonhydrolyzable analog, or drugs were added. The solutions thus modified were applied together with the digitonin, and bathed the cells until the end of the experiment. All experiments were done at 25°C. Results are given ± SE. Latrunculin B was from Calbiochem/Novabiochem (428020), BDM from Sigma, and phalloidin-Texas Red from Molecular Probes.

Microscopy

We used EFM (or TIRFM) to image subsurface regions of cells where cells adhered to a coverslip. To gain free access to the specimen we used "prismless" EFM, a method that has been used successfully to image fluorescent molecules in water (Conibear and Bagshaw, 1996; Tokunaga et al., 1997) and intact cells (Stout and Axelrod, 1989; Steyer et al., 1997). To excite fluorescence, light from an argon laser (488 nm) passed through an objective (Zeiss 100 × 1.4 NA) specially selected for a high numerical aperture, and was constrained by an annulus to the most peripheral portion of the objective's back focal plane. This light is expected to strike the interface between coverslip and cell at a supercritical angle. As discussed previously (Steyer and Almers, 1999) the illumination of cells is only just evanescent. Nonetheless, the intensity of illumination in water declined e-fold within 200 nm from the coverslip, and within 640 nm in the cytoplasm of PC-12 cells (Steyer and Almers, 1999). Measurements confirmed that the secretory granules imaged by us lay at the cell surface (see Results).

Images were captured by a slow-scan air-cooled CCD camera using a 14-bit analog processor (ST-138S, Princeton Instruments) and a back-illuminated imaging chip (SI502BA, Site Inc.). They were analyzed with Metamorph (Universal Imaging Corporation, West Chester, PA). Throughout, fluorescence intensity measurements were corrected for the background measured in a region outside the cell. To determine the fluorescence intensity of individual granules we measured the average intensity in a 300 × 300 nm square placed over the granule center.

Focusing on dense-core granules close to the plasma membrane

Before viewing with EFM, we used reflection interference contrast (RIC, 600 nm light) to focus on the interface between the coverglass and adherent cells. Especially for thin cell extensions (see Fig. 5 *A*, *arrows*) the optimal focal plane for RIC was sharply defined and could be reproduced to within 88 nm by raising and lowering the objective in 100-nm steps with a piezoelectric focusing device. Focusing first with RIC helped to avoid unnecessary exposure of cells to laser light.

When an oil immersion objective looks into water, the objective must be moved by 100 nm to change the focal plane by 88 nm (Majlof and Forsgren, 1993). This correction was applied to all vertical distances except

those corresponding to displacements within the glass coverslip. Strictly speaking, our focal distances are in nanometer water equivalents.

Having focused on the glass/water interface with RIC under red light, how far must one raise the objective to view green fluorescent granules with EFM? In EFM, a green fluorescent bead of 108 nm radius lying on the coverslip had its center 299 nm water equivalents above the RIC image (see Fig. 5 and accompanying discussion). This places the glass-cell or glass-water interface at 299 − 108 = 191 nm water equivalents above the RIC image and corresponds to a mechanical movement of 191/0.88 = 217 nm. To reach the center of a granule 60 nm in radius (Tooze et al., 1991, for our strain of PC-12 cells) one must raise the objective a further 60/0.88 = 68 nm, bringing the total mechanical movement required to 217 + 68 = 285 nm. Our piezoelectric focusing device raised the objective in 100-nm steps. Three steps producing a displacement of 300 nm were assumed to focus on the center of a granule.

Tracking single granules

In most experiments we attempted to track all fluorescent points in a cell that were present in the first image of each recorded sequence. Fluorescent spots representing GFP-labeled granules were tracked over a 1-min sequence of 50 frames, unless the spot was lost from view or coalesced with another spot. Spots that deviated noticeably from being round were excluded because they probably represented clusters of two or more granules too close to be resolved in the *x/y* plane (see the vertical confocal section in Fig. 4 *C*). Because PC-12 cell granules are small, two granules adhering to each other and moving together might still appear as a round single spot, and would not be recognized as a pair. Such pairs, however, were too rare to appear in electron micrographs of two cells (Horstmann, unpublished). Granules that could not be tracked for at least six frames (~15% in an intact cell) were rejected.

Unless indicated otherwise, the location of granules was determined using a program written in C. The program displayed the first image in a sequence, and was then directed by mouse click to the granule of interest. The program found the point of maximum fluorescence within a search circle of 0.3–0.5 μm diameter and selected all pixels around the maximum that exceeded a threshold value for brightness. After excluding bright pixels that were unconnected with other bright pixels, the program determined the center of mass of the fluorescence for the remaining pixels. It then repositioned the center of the search circle over the center of mass, loaded the next frame, and repeated the procedure. The program provided, for each granule tracked, a table of *x* and *y* coordinates as a function of time, representing the projection of the granules' trajectory into the plane parallel to the coverslip.

In some experiments we localized granules by a method that was more laborious, but also more accurate. Images were high-pass filtered at a spatial frequency of 1/μm. We then ran a thresholding algorithm that marked the positions where the fluorescence of granules exceeded a threshold value. We considered a granule's image as a cloud whose thickness represents the local fluorescence intensity. The granule's position was taken to be the cloud's center of mass, determined by an algorithm in Metamorph. It localized the granule to within ~50 nm. The fluorescence intensity of granules was measured on unfiltered images after subtracting a fluorescence background measured outside the cell.

The granule positions thus determined were processed as in earlier work (Qian et al., 1991; Kusumi et al., 1993; Steyer and Almers, 1999). The mean-square displacement (MSD) in the plane of the membrane was calculated for each granule as follows. Assume images are taken at time intervals δt. Let $x(t)$ and $y(t)$ be the coordinates of the granule in one image, and $x(t + n\delta t)$ and $y(t + n\delta t)$ those in another image taken a time interval $\Delta t = n\delta t$ later. Then the square of the displacement during $n\delta t$ is $[x(t + n\delta t) − x(t)]^2 + [y(t + n\delta t) − y(t)]^2$. In each track, the displacement during the interval $n\delta t$ can be measured for $N − n$ intervals, where N is the total number of images in the recording sequence. MSD is the mean of all (N −

n) values, calculated by Qian et al. (1991):

$$\text{MSD}(n\ \delta t) = \frac{1}{N-n}\sum_{j=1}^{N=n}\{[x(j\ \delta t + n\ \delta t) - x(j\ \delta t)]^2$$

$$+ [y(j\ \delta t + n\ \delta t) - y(j\ \delta t)]^2\} \quad (1)$$

where *n* and *j* are positive integers with $n = 1, 2, \ldots (N-1)$. The granule's coordinates at time $j\delta t$ are $\{x(j\delta t), y(j\delta t)\}$ and those a time interval $n\delta t$ later are $\{x(j\ \delta t + n\delta t), y(j\ \delta t + n\delta t)\}$. The MSD was plotted against the time interval Δt, where $\Delta t = n\delta t$.

In some experiments we were interested in the minority of granules that traveled >1 μm in 1 min. Movies of 1 min were analyzed. Images were subdivided into 2×2-μm-square regions and each region was watched several times during playback of the movie sequence. Highly mobile granules were marked and tracked. We counted all granules where the most distant positions on the track were >1 μm apart. Their number was divided by the number of granules in the first image of the sequence.

Microfluorimetric measurement of F-actin content

We treated cells exactly as in experiments involving granule tracking, that is, we permeabilized for 30 s in 7.5 mM digitonin and then waited 90 s, as described earlier. Then we stained for F-actin using two protocols. The first (protocol 1) involved fixation and followed Cramer and Mitchison (1995). Cells were extracted for 45 s in cytoskeleton buffer (Small, 1981) with 0.32 M sucrose, 0.1% Triton X-100, and 1 μg/ml phalloidin-Oregon Green for the stabilization and staining of F-actin. They were then fixed in 4% formaldehyde in cytoskeleton buffer with 0.32 M sucrose for 20 min, rinsed in TBS (Tris-buffered saline, in mM: 150 NaCl, 20 Tris-Cl, pH 7.4), permeabilized by adding 0.5% Triton X-100, and blocked by adding 50 mM NH$_4$Cl. After 10 min, the 50 mM NH$_4$Cl were withdrawn and 0.7 μg/ml phalloidin-Oregon Green were added for further staining F-actin. After 10 min, cells were washed twice for 10 min with TBS plus 0.1% Triton X-100. Cells were then mounted in an open observation chamber and imaged with EFM. For analysis, each cell was outlined and the average intensity within the outline calculated in Metamorph.

The second protocol (protocol 2) avoided fixation. Immediately after a 60-s granule observation period (e.g., in Fig. 11) we permeabilized cells a second time by adding 100 μM digitonin, and included 100 nM phalloidin-Oregon Green in the solution to let us follow the progress of staining. Pictures were taken once every 2 min for 20 min, and analyzed by outlining the cell and plotting its average fluorescence against time. The approach of phalloidin fluorescence to a steady state was fitted with an exponential function (average time constant 7.9 $\pm$ 2.1 min, $n = 50$) whose calculated final amplitude was taken as proportional to the F-actin content pertaining to the end of the granule observation period.

Confocal microscopy

Cells were fixed for 20 min with 3% paraformaldehyde in C-buffer (in mM, 150 NaCl, 5 EGTA, 5 MgCl$_2$, 5 glucose, 10 MES at pH 6.1), quenched for 10 min in PBS (Lang et al., 1997) plus 50 mM NH$_4$Cl, and then washed for 5 min each in PBS and TBS. Cells were delipidated for 1 min in 0.2% Triton X-100 in TBS, incubated thrice (10 min each) in TBS plus 1% bovine serum albumin (BSA), and then stained in TBS plus 1% BSA plus 2.5 μg/ml TRITC-phalloidin (Molecular Probes, 30 min). Cells were washed in TBS plus 1% BSA (10 min), in TBS (10 min) and PBS (10 min), then fixed a second time in PBS plus 3.7% paraformaldehyde (20 min) and quenched in 50 mM NH$_4$Cl. After two washes in PBS (5 min each) cells were put in 90% glycerol and 10% PBS (pH 8.1) for observation in a chamber made from a microscope slide and a coverslip riding on

parafilm spacers. They were examined with a 100×/1.3 Plan Neofluar objective on a LEICA TCS-NT laser scanning confocal microscope (LEICA Microsystems, Heidelberg, Germany). An argon/krypton laser excited fluorescence at 488 nm for GFP and 568 nm for TRITC. GFP and TRITC fluorescence was recorded through 515–545 nm and 585–615 nm band pass filters, respectively. To determine the amount of chromatic aberration in the system, the vertical distance between focal planes for the two fluorescence channels was determined by recording the green and red fluorescence of 220 nm Tetraspeck beads (Molecular Probes, Eugene, OR) in stacks of images taken at 38-nm vertical intervals. The focal length was found to be ~50 nm larger for the red than for the green channel; this small difference was neglected. Point spread functions for the red and green channel were determined from stacks of horizontal (x/y) optical sections (49 nm square voxels) taken at 81-nm z-intervals through 200-nm-diameter TetraSpeck microspheres (Molecular Probes, T-7280).

Horizontal optical sections were imaged simultaneously for red and green channels, and acquired at 162-nm vertical intervals at a lateral voxel size of 65 nm. The two resulting image stacks were each deconvolved with the Huygens2 software (Scientific Volume Imaging, Hilversum, The Netherlands) using the maximum likelihood estimation algorithm (Snyder et al., 1992). The resulting deconvolved stacks were analyzed using the slicer module of the software package Imaris (Bitplane AG, Zurich, Switzerland). This software calculated x/y, x/z, and y/z sections from the image stacks. These were stored in 24-bit RGB TIF format and imported into Metamorph (Universal Imaging Corporation, West Chester, PA) or Adobe Photoshop (Adobe Systems Inc., San Jose, CA).

RESULTS

Both granules and the actin cortex move beneath the plasma membrane

Fig. 1 *A* shows an optical section through the base of a fixed PC-12 cell. Actin-filaments stained red by phalloidin-Texas Red criss-cross the cell, resembling stress fibers. Green dots are sprinkled between them and represent dense-core granules labeled with a fusion protein of human pro-neuropeptide Y and GFP (p-NPY-GFP; Lang et al., 1997). From a stack of such sections at varying vertical planes we reconstructed a section in the vertical plane (Fig. 1 *B*). It shows an actin cortex that is thinnest where the plasma membrane faces the culture medium, and that forms a thick pad where the cell rests on the coverslip. The pad has holes or gaps with dense-core granules inserted into some of them. Apparently granules and actin filaments are in close proximity.

To observe the dynamics of actin and granules in intact live cells, we imaged PC-12 cells by EFM, a technique that images fluorescence preferentially in a 600-nm thin aqueous layer immediately at the coverglass/water interface (Stout and Axelrod, 1989; Steyer and Almers, 1999). The cell in Fig. 2 *A* was transfected with GFP-labeled β-actin (Ballestrem et al., 1998) and shows actin bundles similar to those in Fig. 1. When the bundles were traced and transferred to another image taken 1 min later (Fig. 2 *B*), about half had not significantly changed their location (*arrows*), while others had moved or disappeared. Fig. 3 *A* shows a cell transfected with pNPY-GFP and imaged for 1 min at 0.83 Hz. Fluorescent spots represent single GFP-filled granules. Some moved noticeably, others did not. Fig. 3 *B* shows the tracks of most granules in the horizontal plane. Evi-

FIGURE 1 Location of F-actin and granules at the base of a PC-12 cell. (*A*) Confocal optical section parallel to the coverslip near the bottom of an aldehyde-fixed adherent PC-12 cell. Filamentous actin (F-actin, *red*) was stained with phalloidin-Texas Red, dense-core granules (*green*) were labeled with p-NPY-GFP. (*B*) Reconstruction of a section in the vertical plane (*z*-section) from a stack of 38 optical sections through the cell in *A*, taken at 162-nm vertical intervals. Both lateral and vertical sections were deconvolved as described in Methods.
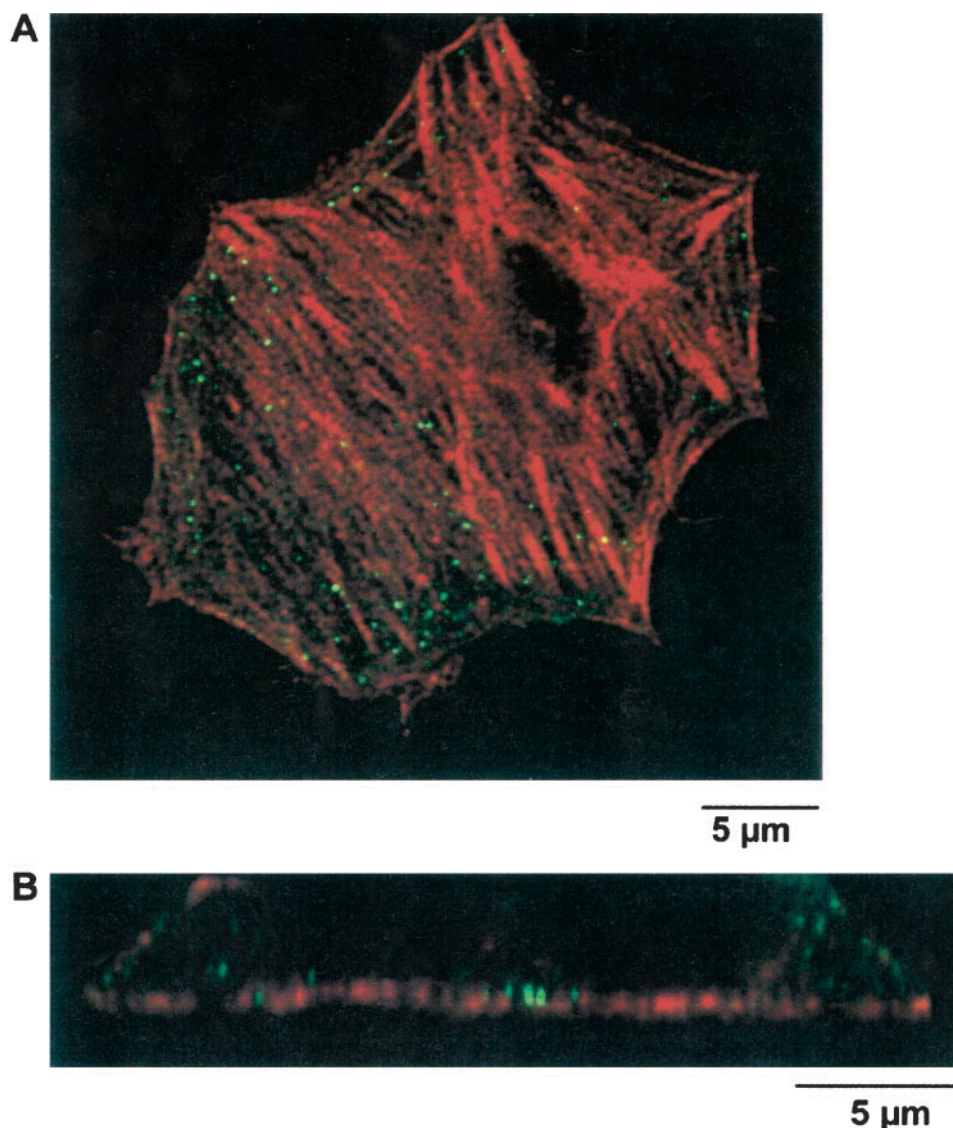
dently both granules and actin bundles move beneath the plasmalemma.

Thickness of the basal actin cortex

To test whether the granules observed in Fig. 3 *A* really do reside in the actin cortex, we first compared the size of granules with the thickness of the cortex in a fixed cell. Portions of Fig. 1 *B* were magnified in Fig. 4, and show the basal actin cortex with granules. Red (Fig. 4 *A*) and green channels (Fig. 4 *C*) are shown separately. Fig. 4 *B* shows a line scan plotting the average brightness of the actin cortex against the vertical coordinate. Brightness is expected to be proportional to the F-actin concentration and exceeded half its maximum value over a 770 ± 20-nm distance in the vertical direction (33 line scans from 2 cells). Fig. 4 *D* shows a line scan through a dense-core granule embedded in the actin cortex. Its half-maximal brightness extended over

only 380 ± 10 nm (40 granules in 2 cells). Actual granules are smaller (120 nm diameter, Tooze et al., 1991) and appear enlarged by blurring due to the limited resolution of our objective. The actin cortex should also be thinner than the 770 nm measured above. However, even if we assume the 380 nm from the granule to arise entirely from blurring as if the granule were infinitesimally small, the actin cortex would still be $770 - 380 = 390$ nm thick. Hence we take 390 nm as a lower bound on the average thickness of the actin cortex sampled as in Fig. 4 *A*. Any granules within 400 nm of the glass coverslip must be embedded in the cortex.

Selective imaging of granules within the actin cortex

What fraction of the granules observed as in Fig. 3 lie within 400 nm of the glass coverslip? Fig. 5 *A* shows a colony of

FIGURE 2 Actin-bundle dynamics in an intact cell. (*A* and *B*) Intact cell in artificial cytosol expressing GFP-β-actin. Streaks of fluorescence represent bundles of F-actin. Actin bundles were traced in *A* and the traces transferred into an image taken 1 min later (*B*). Arrows mark actin bundles that remained in position. Other actin bundles shifted or disappeared.
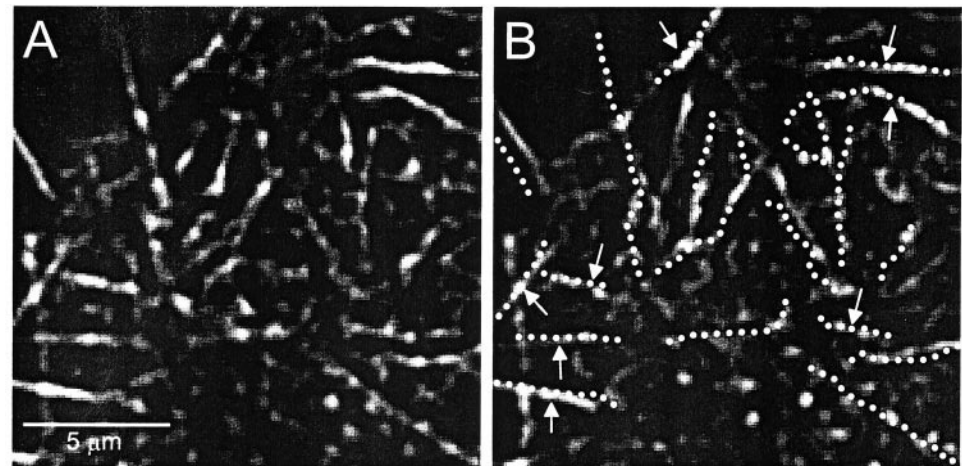
aldehyde-fixed PC-12 cells viewed with RIC. Dark areas indicate regions where the cells adhered tightly to the coverglass (probably within 80 nm; see Steyer et al., 1997) bright regions where adhesion was less (finger-like projections marked by arrows) and gray areas where there was no cell. Living cells gave similar images (not shown). Fig. 5 *A* also shows a bright spot representing a fluorescent bead. The fluorescence excited by EFM was bright enough to appear clearly even against the background of the RIC image. The bead was well outside the cell and hence rested directly on the coverslip. To find its vertical position, we moved the focal plane upward in 88-nm steps. The bead became brighter as it moved into focus and dimmed as the focal plane moved beyond it. At each vertical position we measured the fluorescence where the bead was brightest and plotted the fluorescence intensity against vertical distance. The resulting curve (not shown) showed a peak and was well-fitted by a Gaussian function. The peak of the Gaussian was taken to mark the focal plane through the center of the bead, lying 299 ± 27 nm ($n = 5$ beads) above the focal plane of the RIC image. More importantly, it also marked the position of the interface between the coverslip and the bathing medium. The bead's diameter of 216 nm suggests that this interface lay 108 nm below the center of the bead. In reality, however, the decline of illumination intensity with vertical distance causes peak fluorescence to appear closer to the coverslip than the center of the bead. Hence the coverslip lay <108 nm below the fluorescence peak.

Fig. 5 *B* shows the same cells as in Fig. 5 *A* imaged with EFM. One of them had been transfected successfully, as it showed pNPY-GFP filled granules appearing as fluorescent spots. We determined the vertical position of granules as with the bead, namely by moving the focal plane in 88-nm steps, and at each vertical location measuring the fluorescence intensity of the granule. Fig. 5 *C* plots intensity against vertical distance for two granules with Gaussian curves fitted through the two profiles. One granule (*open circles*) had its center 203 nm above and the other (*filled circles*) 42 nm below that of the glass bead (*upper abscissa*). Because the glass coverslip lay <108 nm below the center of the bead (*lower abscissa*), the centers of the two granules lay <311 nm and <66 nm above the glass coverslip. If the

FIGURE 3 Secretory granule dynamics. (*A*) Intact cell in artificial cytosol expressing pNPY-GFP. The image is the first in a 1-min sequence acquired at 0.83 Hz. Some granules were essentially stationary (*arrow*) while others move apparently randomly (*arrowhead*). (*B*) Tracks of the granules in *A*. The asterisk marks a granule that rapidly moved over relatively long distances.
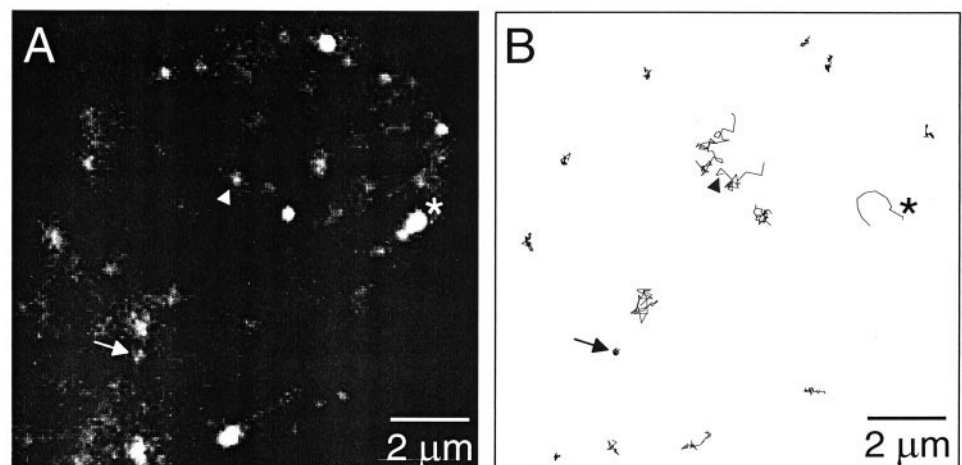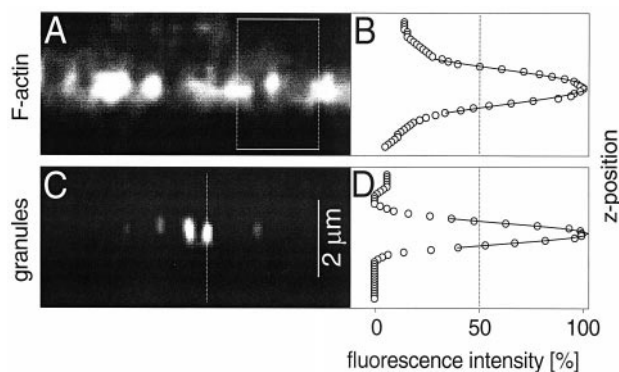
FIGURE 4 Thickness of basal actin cortex. (*A*) Actin and (*C*) p-NPY-GFP fluorescence channels of Fig. 1 *B* separated and magnified. (*B*) 2.1-μm-wide line scan across the basal actin cortex (rectangle in *A*), plotting fluorescence against vertical distance. (*D*) 47-nm-wide line scan through the center of a granule (vertical line in *C*). Granules appear longer in the vertical than the lateral direction because the vertical resolution is relatively lower. Skewed ellipses were excluded (see fluorescent structure to the left of the line in *B*) because they presumably result from two or more granules too close to be resolved.

granule radius was 60 nm (Tooze et al., 1991), the granules were within 251 and 6 nm of touching the coverslip.

The vertical positions of 55 granules from four cells were determined and plotted as a histogram (Fig. 5 *D*). Fifty-two granules had their centers <400 nm above the coverslip, and no granule had its center further than 500 nm; the distance between plasma membrane and visible granules will be less to the extent that an aqueous space intervenes between this interface and the plasma membrane. The analysis suggests that at least 90% of the granules imaged by EFM have their centers within the 390-nm-thick basal actin cortex.

Secretion from the basal actin cortex

As demonstrated in Fig. 3 *B*, the basal actin cortex looks thicker than the actin cytoskeleton in the rest of the cell. To test whether it prevents granules from performing exocytosis, we imaged calcium-triggered secretion of GFP from granules localized in the cell base. Cells were permeabilized with 7.5 μM digitonin, and then placed in a buffer containing either 0.033 μM [Ca^{2+}] or 17 μM [Ca^{2+}]. Cells were imaged repeatedly for 3 min at 0.83 Hz. Exocytosis is expected to diminish the number of fluorescent spots as GFP diffuses out of fluorescent granules. To test for loss of granules, granules in the first (Fig. 6, *A* and *C*) and the last image (Fig. 6, *B* and *D*) of the sequences were counted. At low [Ca^{2+}], the number of granules did not diminish during the 3 min of imaging (to 99 ± 7.4% (*n* = 4); compare Fig. 6, *A* and *B*), whereas in the presence of higher calcium (compare Fig. 6, *C* and *D*) the number of granules decreased to 58.5 ± 5.7% (*n* = 4). In wide-field fluorescence measurements on permeabilized neurites under otherwise simi-

lar conditions, 57% of p-NPY-GFP fluorescence was lost in a calcium-dependent way (Lang et al., 1997).

A likely example of exocytosis is shown in Fig. 6, *E–H*. A granule is shown at various times after [Ca^{2+}] was raised to 17 μM. The moving granule is visible for several frames and then disappears abruptly, as if due to exocytosis (Fig. 6, *G* and *H*). The basal actin cortex apparently allows exocytosis in PC-12 cells, as it does in chromaffin cells (Steyer et al., 1997).

Tracking granules in the actin cortex

Fig. 7 (*top traces*) shows magnified tracks from an experiment as in Fig. 2, except that cells were mildly permeabilized with digitonin. Three types of behavior were seen. A few granules migrated in a directed fashion for micron distances (*A*), but most moved randomly (*B*), and many moved less than our tracking algorithm could detect (*C*). Similar results were obtained in intact cells (Fig. 2). The bottom traces plot the fluorescence intensity of each granule as a function of time. Because our microscope imaged granules with a brightness proportional to their proximity to the coverslip (Steyer and Almers, 1999), changes in fluorescence intensity may be interpreted as vertical motion, i.e., granules brighten as they approach the coverslip and dim as they move away. The granule with the largest motion in the lateral direction (Fig. 7 *A*) also had the largest fluctuations in intensity. When Mg^{2+} was removed and ATP replaced by AMP-PNP, all lateral movement stopped, and intensity fluctuations were always small (compare Fig. 7 *D* and Fig. 7, *A* and *B*).

The movement of most granules is well-described by diffusion

To characterize the movement of granules, we used methods previously established to track single particles (Qian et al., 1991; Kusumi et al., 1993). As an example, Fig. 8 *A* shows results from a highly mobile granule of an intact cell. The *x* and *y* coordinates of the granule were plotted against time and show irregular and possibly random motion. For analysis, we measured the square of the distance traveled by the granule during various time intervals, and plotted the MSD against the time interval (Fig. 8 *B*). Fig. 8, *C* and *D* show a similar analysis for a relatively immobile granule.

If granules moved randomly and with a single diffusion coefficient, plots as in Fig. 8, *B* and *D* should be linear, with a slope equal to four times the diffusion coefficient. Given the large error bars, the MSD plots in Fig. 8, *B* and *D* neither prove nor disprove this idea. To test it further, 61 granules were tracked in an intact cell as in Fig. 2. Ten of the 61 granules could be tracked for at least 44 s, and their MSD plots were averaged. The result was linear, hence the movement of granules is indeed well-described by diffusion (Fig.
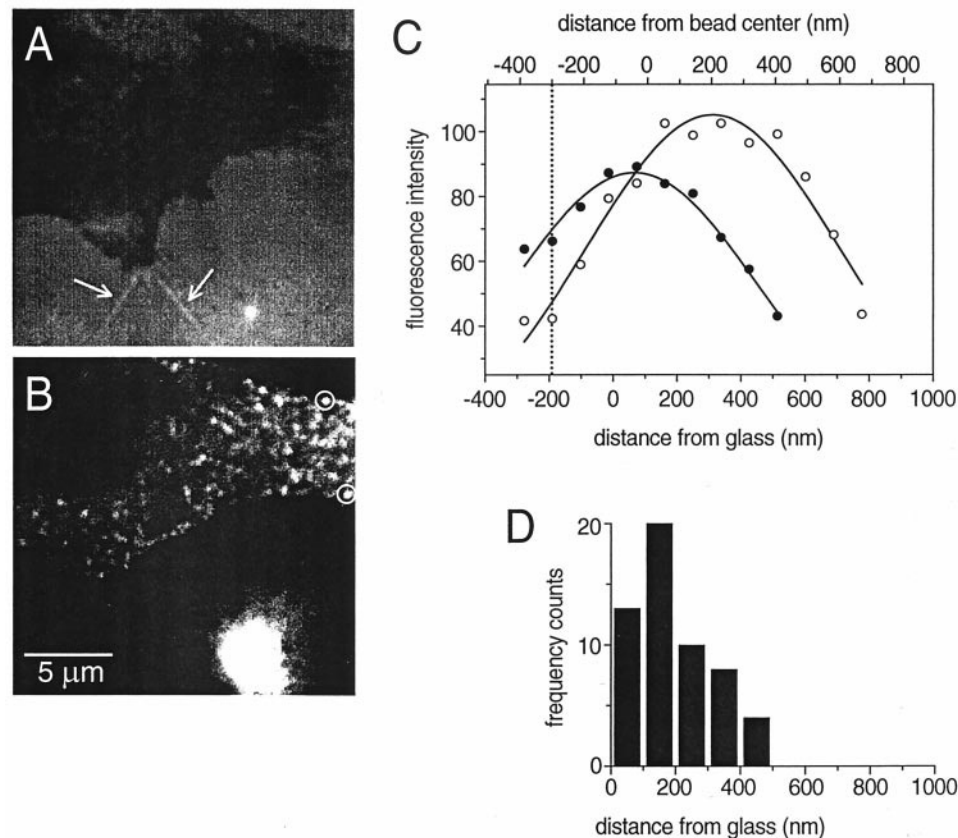
FIGURE 5 Vertical position of granules viewed with EFM. (*A*) Reflection interference contrast image (RIC) of a colony of aldehyde-fixed PC-12 cells. Arrows mark two cell extensions. The small bright spot next to the cell represents a 216-nm-diameter fluorescent bead attached to the coverglass. (*B*) EFM image of the field in *A* showing a p-NPY-GFP transfected cell with punctate granule fluorescence. The white patch toward the bottom is a bead fluorescing ~200 times more brightly than a granule. (*C*) Fluorescence intensity of two granules (*filled* and *open circles*, also marked by rings in (*B*)) against the position of the focal plane. Moving the objective in 100-nm steps moved the focal plane in 88-nm steps (see Methods). As the focal plane moved upward, granules coming into focus brightened and then dimmed again as the focal plane moved beyond them. Gaussian curves were fitted to the two data sets. Their peaks mark the vertical positions where the granule centers are in focus. *Upper abscissa*, distances relative to the focal plane through the center of a 216-nm bead resting on the glass coverslip. *Lower abscissa*, distances from the glass/aqueous interface of the coverslip. Dashed vertical line marks the focal plane of the RIC image, lying 299 ± 27 nm ($n = 5$) water equivalents beneath that of the bead center; this corresponds to moving the objective by 340 ± 31 nm (see Methods). The center of one granule (*filled circles*) was 66 nm, that of the other (*open circles*) was 311 nm above the interface. (*D*) Distances of granule centers from the coverslip; 55 granules in 4 cells analyzed as in *C*.

8 *E*). That granules appear to move randomly does not exclude, however, that they are transported actively.

Mobile and immobile granules coexist

To measure the mobility of individual granules, we determined diffusion coefficients for them by fitting a straight line to MSD plots as in Fig. 8. In intact cells diffusion coefficients varied over a wide range (Fig. 9 *A*). Two-thirds of the granules (47 of 61) moved measurably, while the remainder (*white bar*) moved with a diffusion coefficient $<0.5 \times 10^{-4}$ $\mu m^2/s$, approximately the limit of resolution of our tracking algorithm in these experiments. The mean value for all granules was $23 \pm 5 \times 10^{-4}$ $\mu m^2/s$ (61 granules in 3 cells). Similar results were obtained after cells

were lightly permeabilized with digitonin. Fig. 9 *B* shows a histogram of diffusion coefficients 2–3 min after permeabilization. The mean value was $10.4 \pm 1.8 \times 10^{-4}$ $\mu m^2/s$ (68 granules in 3 cells). After stronger permeabilization (30 s in 100 μM digitonin) the diffusion coefficient was diminished to $2.45 \pm 0.8 \times 10^{-4}$ $\mu m^2/s$ (50 granules in 5 cells). Possibly, cytosolic factors other than Ca^{2+}, Mg^{2+}, and ATP are required for mobility and are lost after strong permeabilization.

We never observed an immobile granule starting to move, neither in intact (14 granules observed for 1 min each) nor permeabilized cells in the presence of MgATP (22 granules observed for 1 min each). Evidently transitions from immobility to movement are rare. Only once did we observe a granule moving for micron distances and then

FIGURE 6 Imaging secretion from the basal actin cortex. Permeabilized cells in 0.037 μM [Ca^{2+}] (*A, B*) or 17 μM [Ca^{2+}] (*C, D*) at the beginning (*A, C*) and end of a 3-min observation period (*E--H*) in 17 μM [Ca^{2+}] showing the movement and disappearance of a granule (marked by an *arrow*), presumably by exocytosis. Times are relative to the disappearance. After permeabilization, cells were either left in the 0.037 μM [Ca^{2+}] artificial cytosol (*A, B*) or stimulated (*A–H*) in a buffer with [Ca^{2+}] = 17 μM (calcium-selective electrode) and [MgATP] = 0.86 mM (calculated). It contained 63 mM potassium glutamate, 50 mM K-EGTA, 49 mM CaCl$_2$, 1.5 mM MgCl$_2$, 1 mM K-ATP, 5 mM glucose, and 20 mM PIPES, pH 7.0). Imaging commenced 30 s after removal of digitonin and continued for 3 min at 0.83 Hz. For quantification of secretion, granules were counted in the first and the last image of sequence.
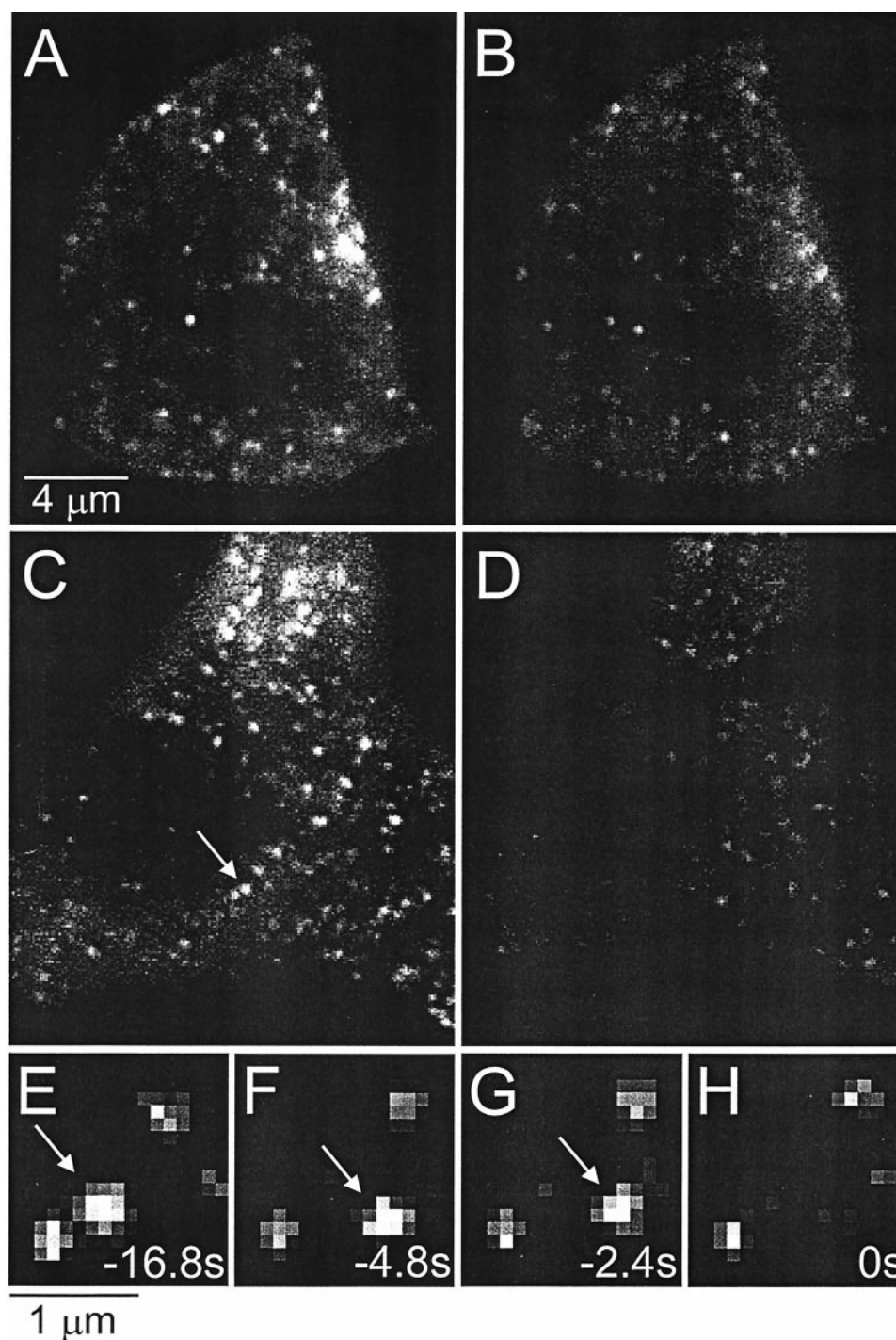
stopping directed motion (Fig. 7 *A*); other highly mobile granules probably left the plane of focus before they stopped moving.

Granules closest to the plasma membrane should fluoresce the brightest as they experience the most intense fluorescence excitation and are the most likely to be precisely in focus. If they are also the least mobile (Steyer et al., 1997), then brightness and immobility would tend to be correlated. Between 13 and 28 granules were tracked in six cells, and both their diffusion coefficient and brightness were measured. To correct for differences in transfection, we calculated the brightness of individual granules as a percentage of the average in each cell. Within each cell, brightness varied over a 4.5 $\pm$ 0.7-fold range ($n = 6$) but was not statistically correlated with the diffusion coefficient ($p < 0.3$, t-test). Evidently, any correlation between prox-
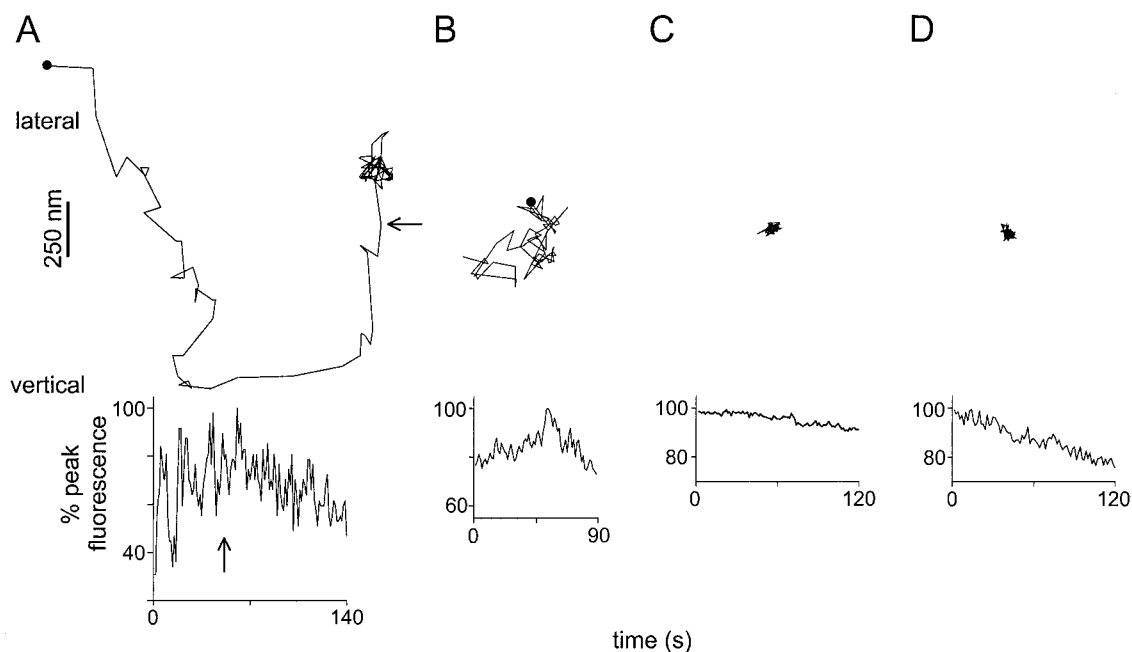
FIGURE 7 Three types of granule movement. *Top:* intensity fluctuations of the granules tracked above represent vertical movements. Throughout, cells were permeabilized, incubated, and imaged (see Methods) in artificial cytosol (*A--C*) or, for *D*, in a modified solution containing, in mM, 63 potassium glutamate, 50 K-EDTA, 5 CaCl$_2$, 1 K-AMP-PNP, 5 glucose, 20 PIPES, pH 7.0. (46 nM calculated free [Ca^{2+}]). Granules were localized with the more accurate method using programming facilities in Metamorph (see Methods).

imity to the plasma membrane and mobility is obscured by variations in granule content of fluorescent GFP.

Directed and random granule movements require MgATP

To test whether motor proteins or ATP-dependent reorganization of the actin cortex may contribute to the motion of granules, we removed free Mg^{2+} with a chelator and exchanged ATP for the non-hydrolyzable analog AMP-PNP. Essentially all movement stopped (Figs. 7 *D*, 9 *C*). The average diffusion coefficient was $0.7 \pm 0.2 \times 10^{-4}$ μm^2/s (68 granules in 3 cells), probably near the limit of resolution of our particle-tracking algorithm. The value can be compared to the diffusion coefficient of $10.4 \pm 1.8 \times 10^{-4}$ μm^2/s (62 granules in 3 cells) in the presence of MgATP (Fig. 9 *B*).

We used a tracking algorithm of greater accuracy (see Methods) to analyze a randomly chosen subset of three granules from each of the six cells on which Fig. 9, *B* and *C* is based. The mean diffusion coefficient with MgATP was $12.9 \pm 4.1 \times 10^{-4}$ μm^2/s ($n = 9$ granules in 3 cells), similar to the mean from Fig. 9 *B*. After MgATP withdrawal, it fell nearly 500-fold to $0.028 \pm 0.017 \times 10^{-4}$ μm^2/s ($n = 9$ granules in 3 cells), at the resolution limit of the method. We also analyzed the fluctuations in fluorescence intensity of granules in this reduced data set. Generally, the fluorescence declined with time due to photo-

bleaching (see Fig. 7, *bottom*). To allow for this, we fitted a straight line to fluorescence traces, calculated the mean-squared deviation from the line, and divided it by the initial fluorescence after subtracting the background. The resulting coefficient of variation was $44.8 \pm 9.2\%$ with MgATP and $4.1 \pm 0.6\%$ without ($n = 9$ granule in 3 cells in each of the two measurements, $p < 0.002$). Evidently, withdrawal of MgATP inhibits both lateral and vertical movements. We next tested three drugs to explore the role of actin and myosin in granule motion.

Degradation of the actin cortex inhibits granule motion

If the actin cortex hindered the movement of granules, then thinning it out should increase granule mobility. This is expected no matter whether granules move by diffusion, by active transport along microtubules, or indeed by any mechanism that does not require actin. Latrunculins disrupt actin filaments in cultured cells (Spector et al., 1983), reduce the viscosity of actin gels from sea urchin egg homogenate (Schatten et al., 1986), and disrupt the yeast actin cytoskeleton within 2 min (Ayscough et al., 1997). Quantitative fluorescence microscopy showed that latrunculin also disrupts the actin cortex in untransfected, permeabilized PC-12 cells (Fig. 10, *A* and *B*), though some actin bundles remain even after treatment with latrunculin (Fig. 10, *C* and *D*); 25
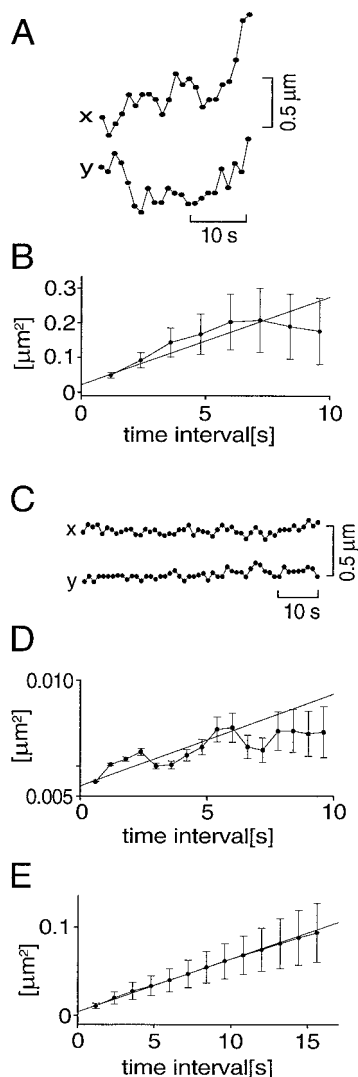
FIGURE 8 Calculation of diffusion coefficients from granule tracks. (*A*) Changes in *x* and *y* coordinates against time (granule indicated by arrowhead in Fig. 2). (*B*) Square of the mean distance moved (MSD) during the intervals shown on the abscissa, calculated from the traces in *A*. Error bars indicate square root of variance, *V*, calculated by $V = \text{MSD}(\Delta t)^2 [2n + 2]/[3(N - n + 2)]$, where *N* is the total number of positions determined, Δt the time interval in seconds, and *n* the time interval in numbers of frames. This equation approximates one derived by Qian et al., 1991 assuming movement to occur with a single diffusion coefficient. To fit the regression line (continuous) each point was weighted by the reciprocal of its variance. Its slope was 0.0252 μm²/s, yielding a diffusion coefficient of 63×10^{-4} μm²/s. (*C* and *D*) As *A* and *B* but for another granule (marked by arrow in Fig. 2). The diffusion coefficient was $0.7 \ 10^{-4}$ μm²/s. (*E*) Averaged MSD values for 10 granules; error bars give SE. Throughout, MSD values were calculated for intervals up to 1/3 the observation time, i.e., for *n* < *N*/3. Intact cells; conditions as in Fig. 2.

μM drug for 2 min diminishes the subplasmalemmal actin content ~10-fold (Fig. 10 *F*).

In parallel experiments, p-NPY-GFP transfected cells were permeabilized and incubated with 25 μM latrunculin present for a total of 2 min. Cells were then imaged to track

granules and diffusion coefficients were measured as in Fig. 8. Contrary to our expectation, the granule mobility approximately halved when the actin cortex was made less dense (Fig. 10 *E*); this result was not changed significantly when we excluded the one granule that moved >1 μm in this data set. Because it is hard to imagine how the actin cortex could fail to be a barrier, the finding suggests that cortical actin itself participates in mediating granule motion.

In particular, the fastest-moving granules (e.g., Fig. 7 *A*) require actin filaments. Cells were permeabilized, exposed to artificial cytosol with or without latrunculin for 1 min, then imaged to watch granule movement for 1 min and stained for F-actin content (protocol 2, see Methods). A total of 50 cells were studied in this way. Among the six cells with the brightest actin cortex (average brightness 1527 ± 84 fluorescence units), none had been treated with latrunculin. A total of 14 granules migrated by long distances (>1 μm in 1 min) at some time or another during each video clip, and there were 459 granules visible in the first images of the six sequences. The ratio, ~3%, is an upper limit for the number of highly mobile granules, since not all granules appearing in a movie are visible in the first frame. Next, the six cells with the dimmest cortex were analyzed (average fluorescence 121 ± 13 units, all treated with 3–12.5 μM latrunculin-B). Only 3 of 494 granules, or 0.6%, migrated >1 μm. Hence, diminishing the cortical actin content by a factor of 12 decreases long-distance movement about fivefold.

BDM and phalloidin inhibit granule motion

Actin filaments could participate in granule motion by providing tracks for the movement of myosins. BDM inhibits the ATPase activity of myosins, but reportedly not of kinesins (Cramer and Mitchison, 1995, but see Krendel et al., 1998), as well as the recruitment of exocytic vesicles to the plasma-membrane in sea urchin eggs (Bi et al., 1997). Cells were permeabilized, incubated for a total of 2 min with 10 mM BDM, and then imaged in the presence of the drug. The diffusion coefficient was three to fourfold lower than in identical experiments without BDM (Fig. 10 *E*), while the density of the actin cortex was not diminished (Fig. 10 *F*). The finding is consistent with a myosin participating in granule movement.

Can granules move within a static actin cortex, or must actin filaments be cut or depolymerized to get out of the way? To test this point we applied phalloidin, a drug that binds tightly and specifically to F-actin (Estes et al., 1981; Vandekerckhove et al., 1985). It stabilizes actin filaments both by preventing monomer dissociation at their ends (Estes et al., 1981; Coluccio and Tilney, 1984; Vandekerckhove et al., 1985; Sampath and Pollard, 1991) and by halving the association rate of monomers at the barbed ends (Coluccio and Tilney, 1984; Sampath and Pollard, 1991). Cells were permeabilized for 30 s with 100 μM digitonin

FIGURE 9 Granule movement requires MgATP. Diffusion coefficients were calculated from granule tracks in the plane of the coverslip. Tracks included up to 50 positions and were rejected if they included <6. White bars represent granules moving with a diffusion coefficient too small to measure with our tracking algorithm. (*A*) Intact cell as in Fig. 2, 61 granules in 3 cells. Symbols indicate diffusion coefficients of three granules in Fig. 3. (*B* and *C*) Permeabilized cells; each panel from 68 granules in 3 cells. (*B*) In artificial cytosol, (C) in an artificial cytosol without MgATP, as in Fig. 7 *D*.
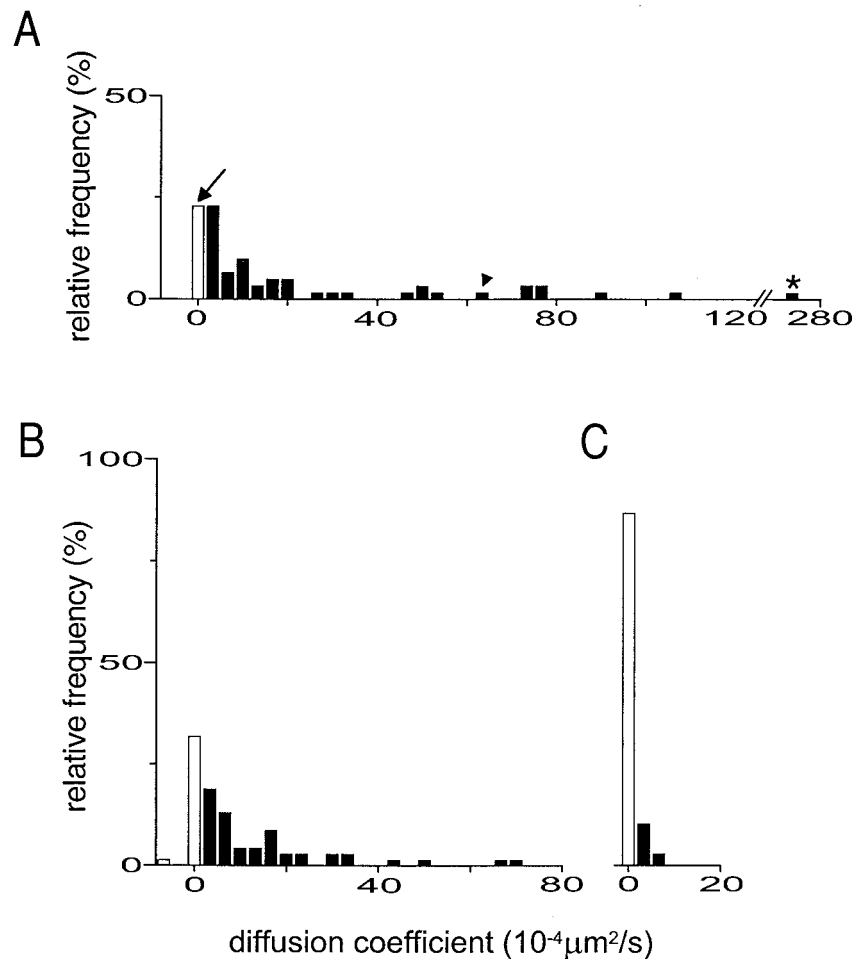
plus 100 nM phalloidin, and then immediately imaged in the presence of the drug. The drug blocked detectable granule motion rapidly and as effectively as did the withdrawal of MgATP (Fig. 10 *E*). In parallel experiments, phalloidin did not significantly change the amount of F-actin in cells (Fig. 10 *F*). Clearly, granule movement requires the continuous remodeling of F-actin, either because granules are passively swept along in a moving actin cortex or because filaments must get out of the way of actively moving granules.

Some granules move along actin bundles

Granules moving passively as a result of F-actin reorganization are not expected to change their position relative to actin filaments nor to migrate along them. To test this point, cells were first watched to track the most mobile granules, and then stained for F-actin with fluorescent phalloidin (protocol 2). Some tracks clearly colocalized with actin bundles (Fig. 11), suggesting that actin bundles can serve as tracks for granules, but coinciding tracks are rare. Their frequency was estimated in a subset of six cells imaged for 1 min each. They contained 14 granules migrating for >1

μm. Two of the 14 paths coincided with actin bundles that appeared after staining (Fig. 11, *A* and *B*), suggesting movement of at least some granules along actin filaments. The remaining 12 tracks did not, either because some granules did not move along actin bundles, because the bundles were too thin to be clearly visible, or because they moved or disappeared (see Fig. 1) before or during the 20-min staining protocol.

DISCUSSION

We have used EFM to observe dense-core secretory granules at the base of living PC-12 cells. The granules imaged by us lay <500 nm above the glass coverslip to which they adhered because our microscope does not image granules further within the cell and/or because granules tend to lie close to the surface in PC-12 cells. Because the actin cortex in our cells extended ~400 nm from the base of an adherent cell, we estimate that ~90% of the imaged granules had their centers within the actin cortex. The actual fraction must be higher since we have not considered that a space exists between the cell and the glass coverslip. Indeed, the
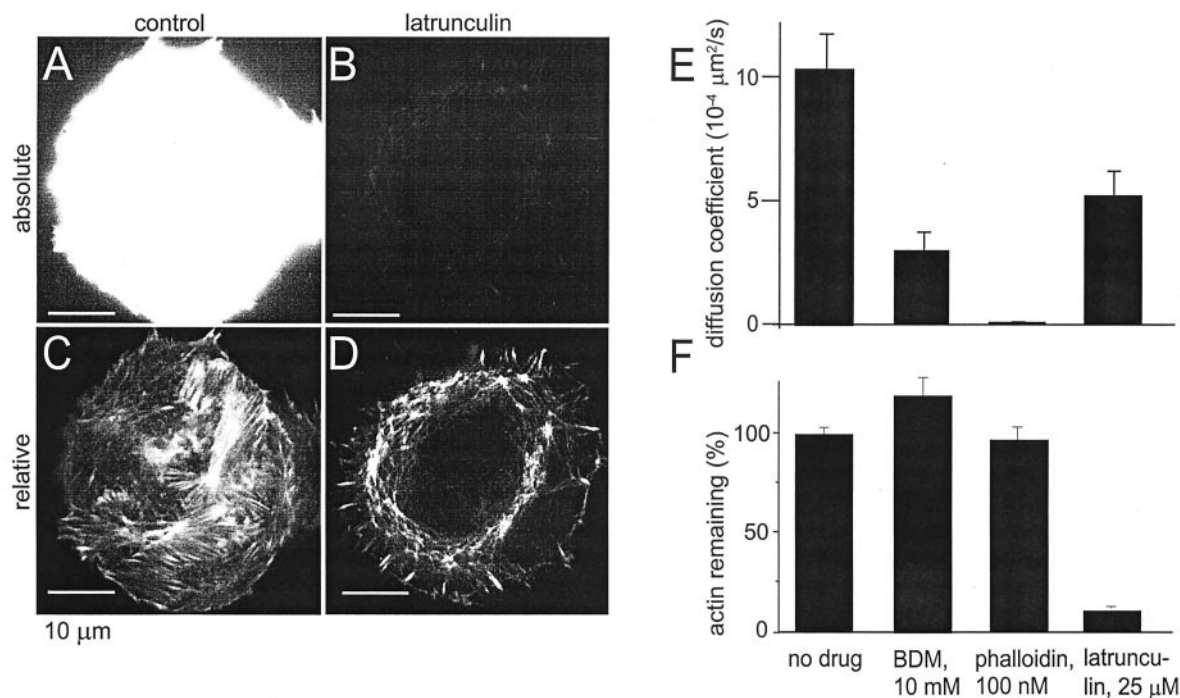
FIGURE 10 Effects of latrunculin-B, BDM, and phalloidin on granule mobility and actin cortex. (A--D) EFM images of untransfected cells. Cells were permeabilized for 30 s, incubated for 90 s, and then fixed and stained with fluorescent phalloidin (see Methods, protocol 1). Permeabilization and incubation without (A) and with (B) 25 μM latrunculin-B. Both imaged at the same brightness. (C) Same view as A at reduced brightness. (D) Same as C at increased brightness to show residual actin bundles. (E) Mean diffusion coefficients of granules in permeabilized cells treated as indicated. In all cases except phalloidin the analysis includes all granules from a cell visible in the first image of the sequence (for each measurement at least 68–105 granules from 3 cells). For phalloidin, cells were more vigorously permeabilized (100 μM digitonin for 30 s). Since granule motion diminished fairly rapidly in this case, the 1-min observation period immediately followed the withdrawal of digitonin. Phalloidin (100 nM) was added as a conjugate with Texas Red. The fluorescence of the conjugate allowed us to verify the access of drug was too weak to obscure the brighter fluorescence from granules. Recordings were made from 5 cells with and 5 cells without phalloidin, and 10 granules/cell were randomly chosen for analysis. The strong permeabilization reduced the diffusion coefficient to $D = 2.45 \pm 0.8 \times 10^{-4}$ μm^2/s, 4.2-fold less than after the usual permeabilization protocol (see Methods). Correspondingly, the bar with phalloidin was scaled up 4.2-fold. (F) Cortical actin content from experiments as in A and B and after treatment with drugs as indicated. For each condition 2 coverslips were imaged (10–20 cells/coverslip). Staining protocol 1. For latrunculin-B, longer incubation times caused little further degradation (to 4.8 $\pm$ 0.1% in 5 min, $n = 16$). In experiments with phalloidin, staining protocol 1 immediately followed a 30-s permeabilization with 100 μM digitonin plus Texas Red-conjugated phalloidin (100 nM).

granules observed by us must be surrounded by actin because all stopped moving when the remodeling of F-actin was inhibited by phalloidin.

In intact and mildly permeabilized PC-12 cells, one-quarter to one-third appeared stationary and moved less than our tracking algorithm could detect. A small minority—<3%—moved in a directed fashion over micron distances, traveling at top speeds of 0.5 μm/s. The remainder appeared to move randomly over smaller distances. In the work by Burke et al. (1997) only one-third of the granules in PC-12 cells were mobile, fewer than in ours. This may be because they studied neurites in NGF-differentiated cells, where granules move more slowly (Kaether et al., 1997) and, perhaps more importantly, because they assayed motion as migration into a bleached area. This method probably would not have detected the small movements registered in granule tracking.

When analyzed by established methods (Qian et al., 1991; Kusumi et al., 1993), the tracks of single granules in the plane of the plasma membrane were found to be well-described by random motion. The mean diffusion coefficient of 10–20 $\times$ 10^{-4} μm^2/s was ~5–10-fold higher than for granules in chromaffin cells ($D = 2.0 \times 10^{-4}$ μm^2/s; Steyer and Almers, 1999) but still 2000–4000-fold less than expected for a 100-nm-diameter sphere in water (4.1 μm^2/s calculated by Stokes' law for a viscosity of 0.851×10^{-3} Ns/m^2). Clearly, the movement of granules is severely restricted, as is the diffusion of other particles in cytoplasm (Luby-Phelps et al., 1987; Jansen et al., 1996).

Movement requires metabolic energy

The random motion of most granules may suggest diffusion as a mechanism. However, some granules clearly move in a
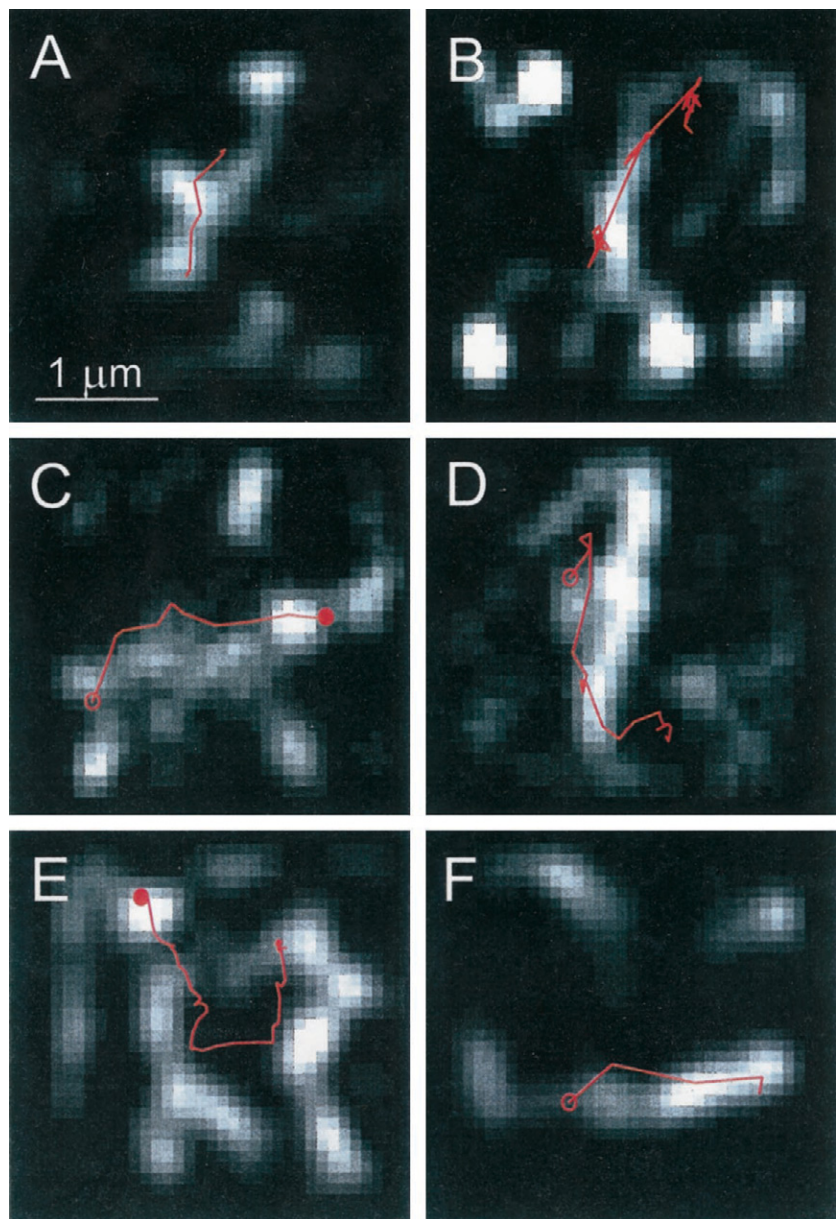
FIGURE 11 Coincidence of migration paths and actin bundles. pNPY-GFP-marked granules were tracked for 1–3 min, then actin filaments were stained with fluorescent phalloidin (protocol 2). Fluorescent granules cannot be seen next to the brighter phalloidin fluorescence. Images *A* and *B* were taken 20 min after admitting phalloidin, and hence 21–23 min after imaging the granules, images *C--F* were taken 5–7 min after imaging and staining.

directed fashion over micron distances both parallel (Figs. 7 *A*, 11) and vertical to the membrane (Steyer et al., 1997). Furthermore, all granule motion stopped when MgATP was withdrawn. With our most sensitive tracking method, granules then had a diffusion coefficient of $<0.03 \times 10^{-4}$ $\mu m^2/s$, or <200 nm/h. Withdrawal of MgATP also slowed or abolished the motion perpendicular to the plasma membrane, as inferred from the decreased fluctuations in fluorescence intensity. Without MgATP, granules apparently do not move.

The ATP requirement may mean that granules are propelled by a molecular motor such as a myosin. Alternatively, the movement of granules may be passive and reflect the movement of the actin around them. The polymerization and depolymerization of actin during actin-driven movement also requires ATP hydrolysis (Alberts et al., 1994). In either case the movement of granules would require metabolic energy.

Inhibition of movement by the myosin inhibitor BDM suggests that ATP is also required to power a molecular motor, and some granules move in a directed fashion as if actively migrating along actin bundles rather than being swept along by actin (Fig. 11). Both results fit with findings that exocytic vesicles contain myosins. Myosin V is found on synaptic vesicles (Prekeris and Terrian, 1997) and myosin I on vesicles that deliver membrane for microvilli (Fath and Burgess, 1993).

The ATP dependence of movement has implications for secretion. A chromaffin cell can release only 3–4% of its catecholamine in the absence of MgATP (Holz et al., 1989),

or ~1000 granules (Parsons et al., 1995). This is closely similar to the number of granules that are docked to the plasma membrane and hence need move no further to perform exocytosis (Parsons et al., 1995; Steyer et al., 1997).

Does actin hinder or mediate the motion of granules?

The actin cortex is often viewed as a barrier that hinders the movement of granules to the plasma membrane (Cheek and Burgoyne, 1986; Sontag et al., 1988; Vitale et al., 1991). Indeed, deep-etch electron micrographs of chromaffin cells show a dense actin network beneath the plasma membrane (Nakata and Hirokawa, 1992) whose mesh size is smaller than the dense-core granule of a PC-12 cell or chromaffin cell. If such a network were not constantly remodeled by depolymerization and repolymerization of F-actin, it would be impenetrable to granules. We found that granule movement stopped when the remodeling of F-actin was prevented by phalloidin or MgATP withdrawal. Hindrance to motion was also apparent in chromaffin cells where chromaffin granules move within a restricted space (Steyer and Almers, 1999). Clearly, the actin cortex can behave as a steric barrier. It is expected to slow the movement of granules and other organelles, no matter whether they move by diffusion, by active transport along microtubules, or by any mechanism that does not require actin.

Surprisingly, granule motion slowed when the actin cortex was degraded by latrunculin. We can imagine only one explanation for this finding, namely that cortical actin filaments not only hinder, but also mediate granule motion. If actin provides tracks for myosin-dependent transport, then every actin filament degraded by an actin-severing enzyme like scinderin (Trifaro and Vitale, 1993) or a drug like latrunculin, removes not only an obstacle, but also a potential track for propulsion. If actin both hinders and mediates motion, then different extents of F-actin degradation may either accelerate or slow movement. This may explain the diversity of effects on secretion observed with actin-depolymerizing treatments, both in chromaffin (Sontag et al., 1988; Morita et al., 1988) and pancreatic acinar cells. It will be interesting to explore whether degradation of the actin cortex in PC-12 cells inhibits or enhances secretion.

Rest and motion in the actin cortex

Many granules fail to move detectably even in the presence of MgATP (Fig. 7 C and Burke et al., 1997). Although some may be bound to the plasma membrane, others are almost certainly bound to the actin cortex. The actin-binding proteins on granules have not been identified. They may include a myosin that binds but no longer moves, being temporarily arrested by a physiologic control mechanism.

Most mobile granules move randomly (Fig. 7 B). If the local environment of a granule is the amorphous actin network, then the interactions between granule and network will be as multidirectional as the filaments that form it. Granules will be pulled in several directions by forces that, through chance synergies, make the pull in one direction temporarily stronger than in others. The pull may come from actin filaments themselves or from myosins crawling along filaments. The direction of movement may change when a filament crossing is reached, when a granule is caught in a mesh it cannot penetrate, or when the random turnover of individual filaments opens channels where before there were none. Hence the network character of the cortex explains why motion is random, while its small mesh size predicts that motion absolutely depends on F-actin turnover.

The rare directed movements over long distances (Figs. 7 A, 11) most probably result from the interaction of a granule with an actin bundle. Filaments in an actin bundle all point in the same direction, giving multiple myosins on a granule the opportunity to pull in that direction. Actin bundles will act much like "thin (actin) filaments," mediating unidirectional movement in striated muscle. Directed movement will continue until the granule encounters and follows another actin bundle (e.g., Fig. 11 E), until it is ensnared in a net of filaments that refuse to depolymerize, or until sufficient myosins bind to other filaments to pull the granule off course.

In summary, three functions of the actin cortex are likely to determine granule motion. First, the cortex forms a steric barrier that would be impenetrable if it were not dynamic. Second, the cortex may move granules by transferring its own movements on them. Third, it provides tracks along which granules are pulled, probably by myosins. All three functions are expected to be subject to physiologic regulation. Possible regulatory mechanisms involve both Ca^{2+} and protein kinase C, which both diminish peripheral F-actin in chromaffin cells (Trifaro and Vitale, 1993; Vitale et al., 1995).

REFERENCES

Alberts, B., D. Bray, J. Lewis, M. Raff, K. Roberts, and J. D. Watson. 1994. Molecular biology of the cell. Garland Publishing, New York. 822–825.

Ayscough, K. R., J. Stryker, N. Pokala, M. Sanders, P. Crews, and D. G. Drubin. 1997. High rates of actin filament turnover in budding yeast and roles for actin in establishment and maintenance of cell polarity revealed using the actin inhibitor Latrunculin-A. *J. Cell Biol.* 137:399–416.

Ballestrem, C., B. Wehrle-Haller, and B. A. Imhof. 1998. Actin dynamics in living mammalian cells. *J. Cell Sci.* 111:1649–1658.

Bi, G-Q., R. L. Morris, G. Liao, J. M. Alderton, J. M. Scholey, and R. A. Steinhardt. 1997. Kinesin- and myosin-driven steps of vesicle recruitment for Ca^{2+}-regulated exocytosis. *J. Cell Biol.* 138:999–1008.

Burke, N. V., W. Han, D. Li, L. Takimoto, S. C. Watkins, and E. S. Levitan. 1997. Neuronal peptide release is limited by secretory granule mobility. *Neuron.* 19:1095–1102.

Cheek, T. R., and R. D. Burgoyne. 1986. Nicotine-evoked disassembly of cortical actin filaments in adrenal chromaffin cells. *FEBS Lett.* 207: 110–114.

Coluccio, L. M., and L. G. Tilney. 1984. Phalloidin enhances actin assembly by preventing monomer dissociation. *J. Cell Biol.* 99:529–535.

Conibear, P. B., and C. R. Bagshaw. 1996. Measurement of nucleotide exchange kinetics with isolated synthetic myosin filaments using flash photolysis. *FEBS Lett.* 380:13–16.

Cramer, L. P., and T. J. Mitchison. 1995. Myosin is involved in postmitotic cell spreading. *J. Cell Biol.* 131:179–189.

Estes, J. E., L. A. Selden, and L. C. Gershman. 1981. Mechanism of action of phalloidin on the polymerization of muscle actin. *Biochemistry.* 20:708–712.

Evans, L. L., A. J. Lee, P. C. Bridgman, and M. S. Mooseker. 1998. Vesicle-associated brain myosin-V can be activated to catalyze actin-based transport. *J. Cell Sci.* 111:2055–2066.

Fath, K. R., and D. R. Burgess. 1993. Golgi-derived vesicles from developing epithelial cells bind actin filaments and possess myosin-I as a cytoplasmatically oriented peripheral membrane protein. *J. Cell Biol.* 120:117–127.

Heumann, R., V. Kacher, and H. Thoenen. 1983. Relationship between NGF-mediated volume increase and "priming effect" in fast and slow reacting clones of PC12 pheochromocytoma cells. Role of cAMP. *Exp. Cell Res.* 145:179–190.

Holz, R. W., M. A. Bittner, S. C. Peppers, R. A. Senter, and D. A. Eberhard. 1989. MgATP-independent and MgATP-dependent exocytosis. *J. Biol. Chem.* 264:5412–5419.

Jansen, R. P., C. Dowzer, C. Michaelis, M. Galova, and K. Nasmyth. 1996. Mother cell-specific HO expression in budding yeast depends on the unconventional myosin myo4p and other cytoplasmic proteins. *Cell.* 84:687–697.

Kaether, C., T. Salm, M. Glombik, W. Almers, and H.-H. Gerdes. 1997. Targeting of green fluorescent protein to neuroendocrine secretory granules: a new tool for real time studies of regulated protein secretion. *Eur. J. Cell Biol.* 74:133–142.

Krendel, M., G. Sgourdas, and E. M. Bonder. 1998. Disassembly of actin filaments leads to increased rate and frequency of mitochondrial movement along microtubules. *Cell Motil. Cytoskeleton.* 40:368–378.

Kusumi, A., Y. Sako, and M. Yamamoto. 1993. Confined lateral diffusion of membrane receptors as studied by single particle tracking (nanovid microscopy). Effects of calcium-induced differentiation in cultured epithelial cells. *Biophys. J.* 65:2021–2040.

Lang, T., I. Wacker, J. Steyer, C. Kaether, I. Wunderlich, T. Soldati, H-H. Gerdes, and W. Almers. 1997. Ca^{2+}-triggered peptide secretion in single cells imaged with green fluorescent protein and evanescent-wave microscopy. *Neuron.* 18:857–863.

Luby-Phelps, K., P. E. Castel, D. E. Taylor, and F. Lanni. 1987. Hindered diffusion of inert tracer particles in the cytoplasm of mouse 3T3 cells. *Proc. Natl. Acad. Sci. USA.* 84:4910–4913.

Majlof, L., and P. O. Forsgren. 1993. Confocal microscopy: important considerations for accurate imaging. *Methods Cell Biol.* 38:79–95.

Merrifield, C. J., S. E. Moss, C. Ballestrem, G. Giese, I. Wunderlich, and W. Almers. 1999. Endocytic vesicles move at the tips of actin tails in cultured mast cells. *Nat. Cell Biol.* 1:72–74.

Mitchison, T. J., and L. P. Cramer. 1996. Actin-based cell motility and cell locomotion. *Cell.* 84:371–379.

Morita, K., M. Oka, and S. Hamano. 1988. Effects of cytoskeleton-disrupting drugs on ouabain-stimulated catecholamine secretion from cultured adrenal chromaffin cells. *Biochem. Pharmacol.* 37:3357–3359.

Muallem, S., K. Kwiatkowska, X. Xu, and H. L. Yin. 1995. Actin disassembly is a sufficient final trigger for exocytosis in nonexcitable cells. *J. Cell Biol.* 128:589–598.

Nakata, T., and N. Hirokawa. 1992. Organization of cortical cytoskeleton of cultured chromaffin cells and involvement in secretion as revealed by quick-freeze, deep-etching, and double-label immunoelectron microscopy. *J. Neurosci.* 12:2186–2197.

Oheim, M., D. Loerke, W. Stuehmer, and R. H. Chow. 1998. The last few milliseconds in the life of a secretory granule: docking dynamics and fusion visualized by total internal reflection microscopy (TIRFM). *Eur. Biophys. J.* 27:83–98.

Parsons, T. D., J. R. Coorssen, H. Horstmann, and W. Almers. 1995. Docked granules, the exocytic burst, and the need for ATP hydrolysis in endocrine cells. *Neuron.* 15:1085–1096.

Prekeris, R., and D. M. Terrian. 1997. Brain myosin V is a synaptic vesicle-associated motor protein: evidence for a Ca^{2+}-dependent interaction with the synaptobrevin-synaptophysin complex. *J. Cell Biol.* 137:1589–1601.

Qian, H., M. P. Sheetz, and E. L. Elson. 1991. Single particle tracking. Analysis of diffusion and flow in two-dimensional systems. *Biophys. J.* 60:910–921.

Sampath, P., and T. D. Pollard. 1991. Effects of cytochalasin, phalloidin, and pH on the elongation of actin filaments. *Biochemistry.* 30: 1973–1980.

Schatten, G., H. Schatten, I. Spector, C. Cline, N. Paweletz, C. Simerly, and C. Petzelt. 1986. Latrunculin inhibits the microfilament-mediated processes during fertilization, cleavage and early development in sea urchins and mice. *Exp. Cell Res.* 166:191–208.

Small, J. V. 1981. Organization of actin in the leading edge of cultured cells: influence of osmium tetroxide and dehydration on the ultrastructure of actin meshworks. *J. Cell Biol.* 91:695–705.

Snyder, D. L., T. J. Schulz, and J. A. O'Sullivan. 1992. Deblurring subject to nonnegativity constraints. *IEEE Trans. Sign. Proc.* 40:1143–1150.

Sontag, J., D. Aunis, and M. Bader. 1988. Peripheral actin filaments control calcium-mediated catecholamine release from streptolysin-O-permeabilized chromaffin cells. *Eur. J. Cell Biol.* 46:316–326.

Spector, I., N. R. Shochet, Y. Kashman, and A. Groweiss. 1983. Latrunculins: novel marine toxins that disrupt microfilament organization in cultured cells. *Science.* 219:493–495.

Steyer, J. A., and W. Almers. 1999. Tracking single granules in live chromaffin cells by evanescent-field fluorescence microscopy. *Biophys. J.* 76:2262–2271.

Steyer, J. A., H. Horstmann, and W. Almers. 1997. Transport, docking and exocytosis of single secretory granules in live chromaffin cells. *Nature.* 388:474–478.

Stossel, T. P. 1993. On the crawling of animal cells. *Science.* 260: 1086–1094.

Stout, A. L., and D. Axelrod. 1989. Evanescent field excitation of fluorescence by epi-illumination microscopy. *Appl. Opt.* 28:5237–5242.

Theriot, J. A., T. J. Mitchison, L. G. Tilney, and D. A. Portnoy. 1992. The rate of actin-based motility of intracellular *Listeria monocytogenes* equals the rate of actin polymerization. *Nature.* 357:257–260.

Tokunaga, M., K. Kitamura, K. Saito, A. H. Iwane, and T. Yanagida. 1997. Single molecule imaging of fluorophores and enzymatic reactions achieved by objective-type total internal reflection. *Biochem. Biophys. Res. Commun.* 235:47–53.

Tooze, S. A., T. Flatmark, J. Tooze, and W. B. Huttner. 1991. Characterization of the mature secretory granule, an intermediate in granule biogenesis. *J. Cell Biol.* 115:1491–1503.

Trifaro, J. M., and M. L. Vitale. 1993. Cytoskeleton dynamics during neurotransmitter release. (Review). *Trends Neurosci.* 16:466–472.

Vandekerckhove, J., A. Deboben, M. Nassal, and T. Wieland. 1985. The phalloidin binding site of F-actin. *EMBO J.* 4:2815–2818.

Vitale, M. L., A. Rodriguez Del Castillo, L. Tchakarov, and J. M. Trifaro. 1991. Cortical filamentous actin disassembly and scinderin redistribution during chromaffin cell stimulation precede exocytosis, a phenomenon not exhibited by gelsolin. *J. Cell Biol.* 113:1057–1067.

Vitale, M. L., E. P. Seward, and J. M. Trifaró. 1995. Chromaffin cell cortical actin network dynamics control the size of the release-ready vesicle pool and the initial rate of exocytosis. *Neuron.* 14:353–363.